Novel O/W nanoemulsions for nasal administration: structural hints in the selection of performing vehicles with enhanced mucopenetration

Emanuela Di Cola[1,2*], Laura Cantù[1], Paola Brocca[1], Valeria Rondelli[1], Giulia C. Fadda[3], Elena Canelli[4], Paolo Martelli[4], Adryana Clementino[5,6], Fabio Sonvico[5,6], Ruggero Bettini[5,6], Elena Del Favero[1*]

[1] Dipartimento di Biotecnologie Mediche e Medicina Traslazionale, Università degli Studi di Milano, via fratelli Cervi 93, 20900 Segrate (Mi), Italy;

[2] Institute Laue-Langevin (ILL), 71 avenue des Martyrs, CS 20156, 38042 Grenoble Cedex 9, France.

[3] Université Paris 13, UFR SMBH, 74 rue Marcel Cauchin, 93017 Bobigny and Laboratoire Leon Brillouin, CEA Saclay F-91191 Gif sur Yvette Cedex, France

[4] Dipartimento di Scienze Medico-Veterinarie, Università di Parma, Strada del Taglio 10, 43126 Parma, Italy

[5] Dipartimento di Scienze degli Alimenti e del Farmaco, Parco Area delle Scienze 27/A, 43124 Parma, Italy

[6] Biopharmanet TEC - Centro Interdipartimentale di Ricerca per l'Innovazione dei Prodotti per la Salute, Parco Area delle Scienze 27/A, 43124 Parma, Italy

*corresponding authors: emanuela.dicola@unimi.it, elena.delfavero@unimi.it

Abstract

We propose novel oil-in-water nanoemulsions (O/W NEs) including PEGylated surfactants and chitosan, showing good biocompatibility and optimization for nasal administration of drugs or vaccines. The transmucosal route has been shown to be ideal for a fast and efficient absorption and represents a viable alternative when the oral administration is problematic. The critical structural features in view of optimal encapsulation and transmucosal delivery were assessed by characterizing the NEs with complementary scattering techniques, *i.e.* dynamic light scattering (DLS), small angle X-ray (SAXS) and neutron scattering (SANS). Combined results allowed for selecting the formulations with the best suited structural properties and in addition establishing their propensity to enter the mucus barrier. To this scope, mucin was used as a model system and the effect of adding chitosan to NEs, as adjuvant, was investigated. Remarkably, the presence of chitosan had a positive impact on the diffusion of the NE particles through the mucin matrix. We can infer that chitosan-mucin interaction induces density inhomogeneity and an increase in the pore size within the gel matrix that enhances the PEGylated NEs mobility. The coupling of mucoadhesive and mucopenetrating agents is shown to be a promising strategy for innovative transmucosal delivery systems.

Keywords: O/W nanoemulsions, porcine gastric mucin, chitosan, small angle x-ray scattering, small angle neutron scattering, transmucosal delivery.

1. Introduction

Nanoemulsions (NEs) are colloidal systems in which the dispersed phase is in the submicron size range. In the pharmaceutical field, the dispersing phase is generally aqueous and the dispersed phase is oily. Pharmaceutically acceptable safe emulsifying agents are available in sufficient concentration to provide stability to the system. NEs are often designed to improve the delivery of specific active pharmaceutical ingredients by their inclusion into different dosage forms (liquids, creams, sprays etc.) for oral, intravenous, intranasal, dermal route administration routes, etc. [1-3]. In this way, water-insoluble drugs can be efficiently dispersed in water because of the lipophilic nature of the discontinuous phase in oil-in-water (O/W) nanoemulsions.

In particular, intranasal administration of NEs has gained increasing interest as a non-invasive administration option to deliver drug systematically [4-6]. Nasal epithelium is better permeable to more diverse and larger compounds (including peptide and proteins) than the gastrointestinal (GI) tract due to the lack of gastric and pancreatic enzymatic activity and the absence of the dilution/interaction effects occurring due to gastrointestinal contents. In addition, NEs are unique vaccine adjuvants since they can elicit an enhanced immune response when mixed with protein antigens. In fact, they are much more than inert vehicles for antigen delivery as they foster the production of robust mucosal immunity, high serum antibodies titres and a cellular immune response through the activation of cytokine production by the epithelial cells and the induction of dendritic cell trafficking [7].

On the other hand, nasal delivery presents some limitations and barriers. Although the available area for drug absorption is relatively large, it is still limited and not easily accessible for large doses of drug. Furthermore, similarly to other mucosal tissues, the nasal mucosa is characterized by the presence of tight junctions and by an abundant mucus secretion. As a consequence, the first barrier encountered by the delivered drugs is the mucus layer. It has been reported that small, uncharged drugs can easily cross the barrier presented by the nasal mucosa, but large, charged molecules have shown lower permeation rates [8-9]. This is principally due to the interactions that particles and molecules can engage with mucins, the main structural components of the mucus gel, which have the tendency to entrap particles and bind to the solutes, hindering their diffusion across the mucus layer. Additionally, the mucociliary clearance, i.e. the continual propulsion of the mucus towards the nasopharynx by ciliated cells, tends to remove entrapped foreign materials, including formulations, from the nasal surface [10].

The NE efficacy, in terms of rate and extent of nasal mucosa contact time and absorption, can be enhanced by the addition of mucoadhesive agents, such as natural biopolymers. Particularly, chitosan (CS) has been largely used as muco-adhesive agent due to its peculiar biological and physico-chemical properties [11-14]. Its polycationic nature allows for electrostatic interaction with the negatively charged mucin glycoproteins, enhances the adhesion to the mucosa and ultimately increases the contact time of the drug formulation with the mucosal surface, improving bioavailability. Furthermore, CS acts also as penetration enhancer through the reversible opening of tight junctions between epithelial cells, thus promoting paracellular drug transport [15]. Therefore, the local biological environment and the permeability of the mucosa can be modulated to ease drug permeation, by using the proper formulation design. Several studies have been devoted to the interactions between CS and

mucins, showing that in aqueous environment the electrostatic attraction is not the only force driving the association between these two biomolecules, but hydrogen bonding and hydrophobic forces also contribute [16-17]. Up to date, comprehensive studies on the mechanisms underlying mucoadhesion have been carried with methods testing directly for interactions at a macroscopic level [18] or based on the rheological properties [19-20]. Detailed structural studies of the interactions of muco-adhesive biopolymers with mucins at macromolecular level in the bulk are still lacking. In this context, Menchicchi *et al.* tested a series of polysaccharides and their interaction with partially purified porcine gastric mucin as a first step toward the rational design of mucoadhesive polysaccharide-based nanoformulations [21], while Haugstad *et al.* [22] studied the comparison of the interactions between alginates and CS with mucins by atomic force microscopy.

Here, the mucoadhesive properties of CS and its role in modulating the diffusion of nanocarriers inside the mucus matrix were investigated in the framework of novel O/W NE formulations designed for nasal administration. To this scope, we employed complementary scattering techniques, *i.e.* dynamic light scattering (DLS), small angle X-ray (SAXS) and Neutron scattering (SANS). Scattering techniques at large-scale facilities offer the unique advantage of a detailed structural inspection with high resolution over a wide range of length scale [23], thereby allowing a deeper insight into the mechanisms of CS mucoadhesion. The interaction of the NEs with mucin gels was investigated by comparing formulations with and without CS. Commercial porcine purified mucin (PGM) was chosen as mucus model, although only partially reproducing the complex composition, structure and transport properties of native mucus. In fact, the highly variable composition of collected native mucus would prevent a reproducible interpretation of experimental results aimed at identifying the basic carrier-mucus interactions during particle diffusion. Pig and human mucus display similarity in structure and molecular weight; mucin glycoproteins can be purified in bulk from native porcine gastric mucus and reconstituted mucin hydrogels have been successfully established [24-25].

All the investigated NEs are formulated with a PEG coated inert surface [26] aimed at avoiding entrapment by the mucus barrier. Moreover, CS was not chemically grafted onto the nanoparticle surface but it was used as a mucus-modulating agent in co-association with the nanoformulation. This strategy allows bringing modification to the mucosal barrier without requiring complex and expensive surface engineering [27]. Our results show that CS modifies mucin-mucin interactions, while still preserving the overall architecture of the matrix. The outcome is an increase in the pore size within the gel matrix that enhances the nanoparticle mobility across the mucosal barrier and eventually improves functional drug therapy.

2. Materials and Methods

Commercial porcine gastric mucin (PGM type II, bound sialic acid <1.2 %) was purchased from Sigma Aldrich (St. Louis, USA). Chitosan (ChitoClear® FG95 LV, PRIMEX, Siglufjourdur, Iceland) was used. The TM1703 batch has a molecular weight of approx. 30 kDa, viscosity of 8 cPs at 1% w/v in acetic acid (1% w/v), and 99% degree of deacetylation. Ph.Eur. and USP monographs compliant PEG-12 15 hydroxystearate (Solutol® HS 15), macrogolglycerol ricinoleate (Cremophor® EL) and D-alpha-tocopheryl polyethylene glycol succinate

(Kolliphor® TPGS) were kind gifts from BASF AG (Ludwigshafen, Germany). Sunflower oil and vitamin E (DL-alpha-tocopherol) were purchased from A.C.E.F. S.p.A. (Fiorenzuola d'Arda, Italy). Particulate free ultrapure water (0.055 µS/cm, TOC 1 ppb) was obtained with a Purelab Pulse Flex Ultra-pure water system (Elga Veolia, Milan, Italy). All other reagents were of analytical grade and used as supplied.

Three CS-added NEs were prepared by a low energy emulsification method (**Experimental** of **Appendix A**). The weight-fraction composition of the final NEs was the following: 80% CS aqueous solution, 10% emulsifying agent, 5% sunflower oil, 5% α-tocopherol (w/w).

SAXS was performed at the beamline ID02 of the European Synchrotron (ESRF, Grenoble, France) [28], while SANS was carried at the Laboratoire Leon Brillouin (LLB, Saclay, France) on the PACE spectrometer [29]. The detailed description of the techniques is reported in **Experimental** of **Appendix A**.

3. Results

3.1 Structure of the O/W nanoemulsions (NEs)

In the following, the structural analysis of the O/W NEs by means of SAXS is detailed. As specified in **Methods**, the three formulations have a similar basic by-weight composition, and differ in the type of PEG-conjugated emulsifier. SAXS measurements were performed in two different conditions, without and with added CS.

3.1.1 Vitamin E TPGS-based O/W NEs

The first type of NE investigated is based on Vitamin E TPGS (Kolliphor), a non-ionic surfactant formed by the esterification of vitamin E succinate with polyethylene glycol (PEG) 1000 (see **Table A.1** in **Appendix A** for the details on the chemical composition and scattering length densities (SLD) [30-31]).
TPGS is largely used as an emulsifier or as an ideal coating molecule for fabricating drug-loaded nanoparticles with high encapsulation efficiency and cellular uptake, thus improving therapeutic effects [30]. In **Fig. 1A** the scattering patterns $I(q)$ from 4% w/v solutions of TPGS NEs are shown, with and without added CS.
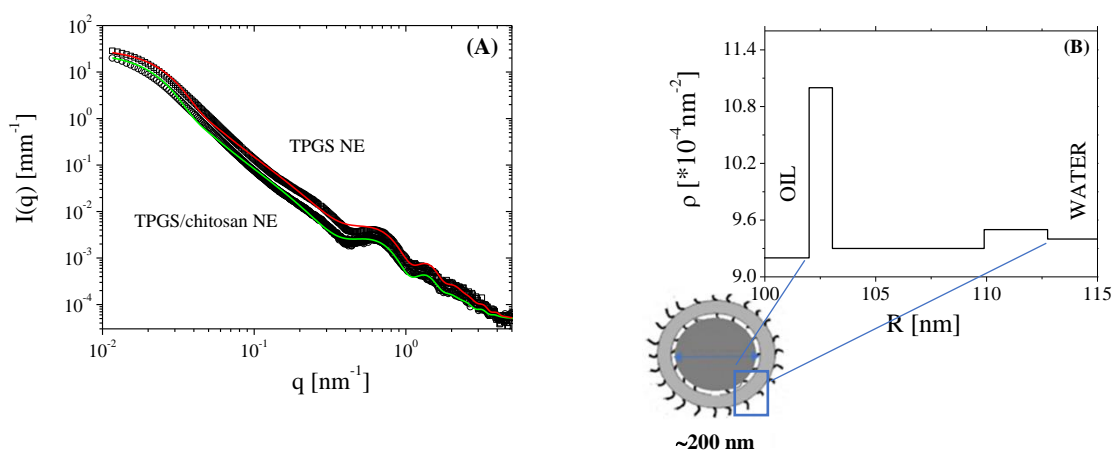
Fig. 1. **Panel A**. The comparison between SAXS intensity profiles of TPGS-based O/W NEs, at c = 4% w/v: CS-added (c = 0.03% w/v, squared symbols) and CS-free (open circles symbols). The solid lines represent the best fit to the spherical core-shell model (n_{shell} = 3) of eqs (**2**) and (**3**) **Panel B.** Sketch of the NE highlighting the SLD profile (ρ) of the wrapping bilayer.

At first glance, the overall structure in the two cases is similar, in agreement with the DLS results, which indicate that the hydrodynamic size is unchanged upon the addition of CS (R_h ~126 nm).

The SAXS background-subtracted scattered intensity $I(q)$ can be expressed as:

$$I(q) = NV^2 \Delta\rho^2 P(q)S(q) \quad \textbf{(1)}$$

where N is the number of particles per unit volume V, $\Delta\rho$ is the different in the scattering density between the particles and the medium, $P(q)$ and $S(q)$ are the form factor and the structure factor, describing the shape and interaction between particles, respectively [32-33]. In the specific case, we can safely neglect interparticle interactions, i.e. $S(q) \approx 1$, and $I(q)$ can be best modelled using the $P(q)$ of a core-shell droplet, calculated according to eq. (**2**) (**Fig. 1A,** solid lines).

$$P(q) = \left[V_c(\rho_c - \rho_s) \frac{\sin(qR_c) - qR_c\cos(qR_c)}{(qR_c)^3} + V_s(\rho_s - \rho_m) \frac{\sin(qR_e) - qR_e\cos(qR_e)}{(qR_e)^3} \right]^2 \textbf{(2)}$$

V_c and V_s indicate the volumes of core and shell, R_c the radius of the core, R_e is the external radius, and ρ_c, ρ_s ,ρ_m are the scattering length densities of the core, shell and solvent. In our case, the shell was treated as a multi-layered shell with uniform SLD, considering the scattering from the acyl-chain and headgroup regions separately [34]:

$$\rho(x) = \begin{cases} \rho_1 & R_c < x < R_c + t_1 \\ \rho_2 & R_c + t_1 < x < (R_c + t_1) + t_2 \\ \rho_3 & R_c + t_1 + t_2 < x < (R_c + t_1 + t_2) + t_3 \end{cases} \quad \textbf{(3)}$$

where ρ_1 and ρ_3 refer to the head group regions on both sides of the middle hydrophobic chains (ρ_2). t_i (i=1-3) is the size of the layers. The polydispersity was only considered for the core region, using a Schulz type size distribution [35].

The peculiar "onion-like" shape is due to the high TPGS surfactant fraction, which exceeds the minimum amount necessary to stabilize the actual hydrophobic core (R_c ~100 nm). TPGS molecules, besides surrounding the core with a monolayer, insert their hydrophobic tails into the oil, and form an additional bilayer envelop where a hydrophobic region (vitamin-E succinate) with a thickness of about 7 nm is sandwiched between two layers of PEG. Its contrast profile is reported in **Fig.1B** [see **Table A.2** of **Appendix A** for fit parameters]. Notably, the two PEG layers are very different. On the inner side, PEG is close-packed in a thin 1 nm crust, while on the outer side, the PEG brush thickness is of the order of ~3 nm, compatible with the length of

extended highly hydrated PEG chains [36]. The detailed SAXS description of the NE particles reveals that, despite the abundance of TPGS-emulsifier, an improved fragmentation of the oil phase could not be attained, since TPGS forms an over-coverage of quite large particles rather than stabilizing a higher number of smaller particles. The addition of CS to the solution does not affect the overall particle architecture and no dramatic changes in the external shell are observed, indicating that only weak interactions are engaged between PEG and CS chains.

3.1.2 Macrogolglycerol ricinoleate-based O/W NEs

The second formulation is based on macrogolglycerol ricinoleate (Cremophor EL), a non-ionic surfactant prepared by reacting ethylene oxide with castor oil in a molar ratio 35:1, which is used as a vector for the solubilization of a wide variety of hydrophobic drugs [37]. The SAXS intensity profiles of NEs with and without added CS are compared in **Fig. 2A**. Here, contrary to TPGS-based O/W NEs, structural changes are observed upon the addition of CS. The overall scattering signal was fitted using a 2-level model with spherical core-shell primary particles (eq. (**2**)), clustered in larger assemblies via polymer inter-chain networks. In CS-added NE, a steeper slope in the low-q region (upturn at $q < 0.03$ nm^{-1}) indicates that clusters are larger as compared to CS-free NEs. The cluster contribution to the SAXS intensity can be described with a Debye-Anderson-Brumberger (DAB) term $S_c(q)$:

$$S_c(q) = \frac{I_M}{(1+\Xi^2 q^2)^{d_f}} \quad (6)$$

I_M and Ξ are proportional to the average mass and the characteristic size of the clusters [($\Xi^2 \approx R_g^2/6$), being R_g the radius of gyration of the clusters], respectively. d_f is a power law exponent related to the fractal cluster dimension. In the CS-free NE, Ξ is ≥ 67 nm and d_f ~2, while in the CS-added NE, Ξ is found ≥ 80 nm with d_f ~1.8. The fractal dimension suggests in both cases a moderately ramified distribution of the NE particles (branched aggregates) [see **Table A.3** of **Appendix A** for fit parameters].

On the other hand, in the intermediate q-range the scattering patterns of CS-added and CS-free NE overlap, suggesting that the primary particles (individual droplets) are mainly preserved ($R_{primary}$ between 7 and 8 nm). Thus, the total intensity, including the single-particle and the cluster term is given by [38]:

$$I(q) = N_p \Delta\rho^2 V_p^2 P(q)[S(q) + S_c(q)] \quad (7)$$

where $S(q)$, the droplet-droplet interaction, is ≈ 1 and $P(q)$ is the form factor contribution from the individual core-shell particles.

3.1.3 PEG-12 15 hydroxystearate-based O/W NEs

The last formulation is an O/W NE based on poly(ethylene glycol) 15-hydroxystearate (Solutol). In similar systems [39], colloidal suspensions with large droplet size ($R_h > 120$ nm) are formed for a surfactant/oil weight ratio lower than 2.5. In the present case, being the surfactant-to-oil ratio about 2, a colloidal dispersion of large particles ($R_h \sim 98$ nm) is indeed observed by DLS analysis. **Fig. 2B** shows the SAXS patterns of the Solutol-based NEs with and without added CS.
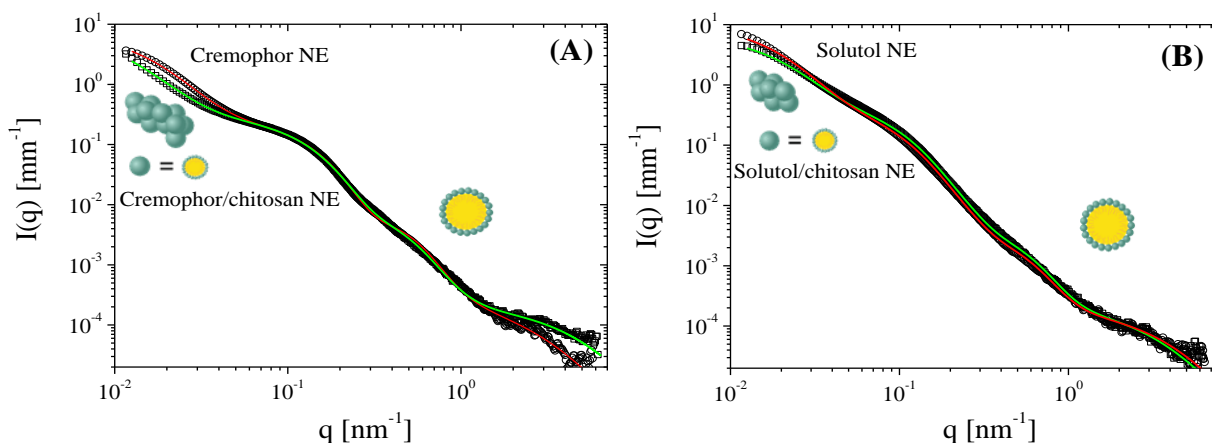

Fig. 2. The SAXS intensity profiles of NEs, $c = 4\%$ w/v CS-free (open squares) and CS-added ($c = 0.03\%$ w/v, open circles). (**Panel A**) Cremophor-based NEs. (**Panel B**) Solutol-based NEs. The solid lines correspond to the best fit to eq (**7**). The excess scattering in the low-q region was fitted according to eq. (**6**)

Alike Cremophor-based NEs, these systems adopt a spherical droplet sub-structure, with an oily core stabilized by PEG 660-stearate chains at the surface, sterically preventing droplets from coalescence. The size of such primary particles is about 12 nm. On the large length scale (low-q region), an excess scattering indicates large assemblies of primary particles interconnected via PEGylated chains, with an average size R_g of ~110 nm and mass fractal exponent $d_f \sim 1.8$ (ramified aggregates). Contrary to Cremophor-based NEs, the size of Solutol-based NEs clusters is lower ($R_g \sim 102$ nm) in presence of CS, the shape of the primary nanoparticles being unchanged. The zeta potential turns from negative (~-24 mV) to positive (~+12 mV) [see **Table A.3** of **Appendix A** for fit parameters], in analogy to Kolliphor- and Cremophor-based NEs, confirming that electrostatic interactions occur between CS chains and the surface of the NEs. Nonetheless, CS is seen to hinder droplet clusterization in this case. SAXS results, obtained at $c = 4\%$ w/v, agree with DLS analysis, performed at a much lower concentration, namely $c = 0.04\%$ w/v. In the very dilute condition, clusters of primary particles are also observed although smaller and their size is found to reduce from ~98 nm to ~67 nm when CS is added.

Table 1

Results from the structural characterization of the O/W NEs by complementary methods: Zeta potential, DLS* (R_h, *overall concentration $c = 0.04\%$ w/v) and SAXS** ($R_{primary}$, $R_{g \, cluster}$, **overall concentration $c = 4\%$ w/v).

O/W NE	Zeta potential [mV]	R_h* [nm]	$R_{primary}$ ** [nm]	$R_{g\ cluster}$** [nm]	Model
Kolliphor-based NE	-24.4 ± 7.3	126 ± 2	≥ 74	-	core-shell (*n*=3 shells) spherical particles
Kolliphor-based NE + CS	*+8.0 ± 7.2*	*127 ± 2*	*≥74*	*-*	
Cremophor-based NE	-28.9 ± 5.0	50 ± 2	7±2	≥147	ramified 2-level structure / spherical primary particles
Cremophor-based NE + CS	*+9.8 ± 5.6*	*59 ± 12*	*8±2*	*≥196*	
Solutol-based NE	-24.7 ± 5.9	98 ± 3	12±4	≥110	ramified 2-level structure / spherical primary particles
Solutol-based NE + CS	*+11.8 ± 0.5*	*67 ± 7*	*12 ± 4*	*≥102*	

It has been shown that the molecular architecture of electrostatic complexes between nanoparticles and bio-polyelectrolytes strongly depends on the interplay between the polyelectrolyte intrinsic rigidity (persistence length, L_p) and the nanoparticles size (R) [30]. The ratio L_p/R is the main tuning parameter controlling the fractal dimension d_f of the nanoparticles self-assemblies. CS is considered as a semi-flexible polyelectrolyte with a persistence length of ~ 9 nm [40]. At high ionic strength (Saline Simulated Nasal Fluid (SSNF), $k^{-1} < 1$ nm, composition in **Appendix A**) the parameter L_p/R is of the order of 0.1 for both Cremophor-based and Solutol-based NEs. In both cases, we observe the formation of complexes with CS, displaying branched structures similarly to what observed in complexes of CS with silica nanoparticles [41].

The results in **Table 1** highlight the peculiar structure of the Kolliphor-based NE as compared to the other two systems, i.e. the oil phase cannot be fragmented beyond a certain extent and the solute units are individual mono-core large stabilized droplets. On the contrary, in both Cremophor-based and Solutol-based NEs, the solute units are coordinated multi-core clusters containing smaller droplets, that can be both transported as a netted ensemble and eventually delivered as individual subunits, still maintaining their individual stability.

3.2 Interactions between NEs and porcine gastric mucin (PGM)

As a further step, the above characterized NEs were studied for their interaction with mucin, the main glycoprotein of the mucus. Indeed, beside size-limitation imposed to drug delivery by the pore size of the mucus mesh (*size-exclusion barrier*), the diverse domains of mucin molecules provide several *loci* of interaction with both hydrophilic and hydrophobic incoming particles (*interaction barrier*) [9]. Here, the physico-chemical properties of mucin as an interaction barrier were investigated by SAXS. The mucin matrix was previously characterized and then mixed with the above described NEs.

3.2.1 Porcine gastric mucins (PGM) in SSNF

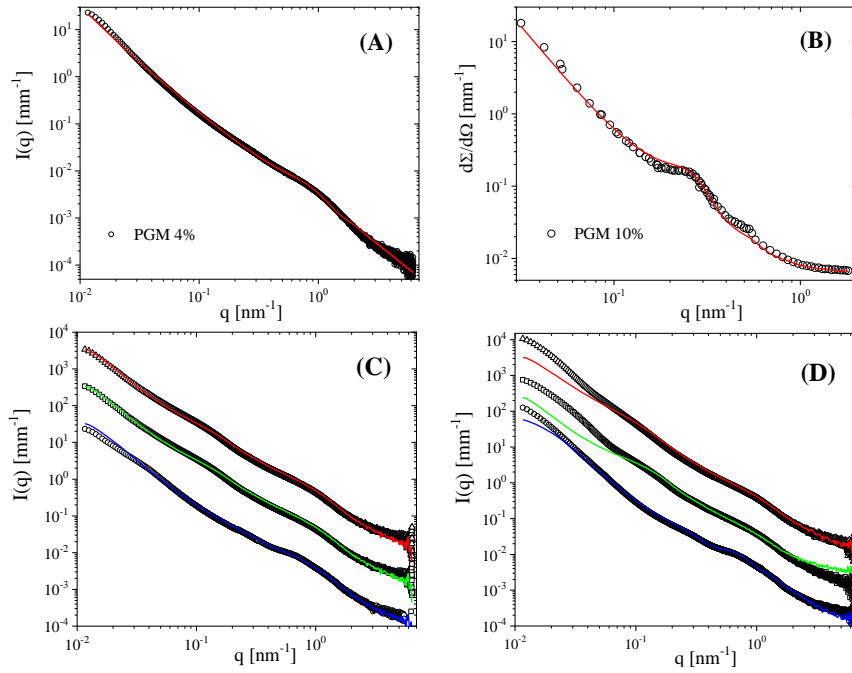The SAXS scattering pattern from the solution of PGM ($c = 4\%$ w/v in SSNF) is shown in **Fig. 3A**.

Fig. 3. (**Panel A**) SAXS intensity spectrum of PGM at $c = 4\%$ w/v in SSNF (symbols). The full line is the fit according to the revisited dumbbell model [42-45], eq. (**8**): $R = (9.2\pm0.3)$ nm, $\xi = (23\pm2)$ nm and $\Xi \geq 90$ nm. (**Panel B**) SANS scattering profile of solution of PGM at $c = 10\%$ w/v. The full line corresponds to the fit to eq. (**8**), with similar parameters of SAXS. Intensity maxima are due to the locally ordered hydrophobic-end globular cysteine-rich regions of the protein. (**Panel C, D**) SAXS intensity profiles of CS-free NEs (**Panel C**) and of CS-added NEs (**Panel D**), in interaction with PGM at equal concentration ($c = 4\%$ w/w) and volume (1:1 v/v): TPGS (open circles, bottom), Cremophor-EL x 10 (open squares, medium), Solutol x 100 (open triangles, top). The solid lines represent the reconstruction of the scattering signal of the mixture by the linear combination of the scattering signal of the individual components.

The estimated Debye screening length of the solution was ∼0.37 nm, smaller than the correlation length of the carbohydrate side chains along the protein peptide backbone (size of brushes ∼1-2 nm). Therefore, mucin chains adopt a random coil flexible conformation at neutral pH. The non-glycosylated cysteine-rich regions of mucin fold to hide the hydrophobic domains, forming globules stabilized by salt bridges between the anionic carboxylates and the cationic amino groups [42]. Due to its complex conformation, the mucin structure has been described by different models [41-44]. Here, the overall scattered intensity profile was fitted using a dumbbell-shape form-factor [44-45].

$I(q) = I(q)_{\text{peptide}} + I(q)_{\text{globule}}$ (**8**)

Where

$$I(q)_{peptide} = \frac{I_1}{\xi^2 q^2} + \frac{I_2}{\Xi^n q^n} \quad (\mathbf{9})$$

and

$$I(q)_{globule} = NV^2(\rho_m - \rho_s)^2 P(q) S_{P-Y}(q) \quad (\mathbf{10})$$

Being $P(q)$ and $S_{P-Y}(q)$ the form and structure factor (hard sphere with Percus-Yevick closure) of polydisperse interacting spheres ($R\sim10$ nm), respectively [44].

The dumbbell model gives the overall scattering intensity $I(q)$ as the sum of two different contributions: one generated by the flexible peptide backbone, $I(q)_{peptide}$, and the second coming from the interference between the globular end-regions, $I(q)_{globule}$. From the model, we estimated the characteristic length of the peptide backbone $\xi\sim23$ nm, acting as a glycosylated spacer, consistent with what previously reported in the literature [44-45]. Concerning the size of the mucin clusters, only a lower-limit Ξ can be estimated from the available q-range ($\Xi \geq 90$ nm). The Porod exponent was found 2.7, as expected for polymeric networks with a mass fractal structure [38]. In **Fig. 3B,** the SANS scattering profile from a solution of mucin in SSNF ($c = 10\%$ w/v) is also shown for comparison. The best fit to the experimental data has been obtained with similar parameters as for the SAXS spectra. As compared to SAXS, SANS investigation of PGM in solution gives better visibility to the interference between the hydrophobic globules connected by the glycosylated peptide backbone, thus showing pronounced maxima in the scattering pattern. The position of the first peak corresponds to the characteristic interchain distance (~25 nm) between the locally ordered hydrophobic globules (concentrated dispersion of uncharged (polydisperse) spheres) [44].

3.2.2 Mixtures of O/W NE and PGM (1:1 v/v)

In **Fig. 3C,** the SAXS spectra from the CS-free NEs in interaction with PGM are analyzed by comparing them with the scattering signal obtained by the linear combination of the SAXS profiles of the single components, i.e. NE and PGM (solid lines). For all of the three investigated systems, such procedure allows reconstructing the signal from the mixture over the whole q-range. In the case of Solutol-based and Cremophor-based NEs, the fit parameters indicate that NEs and PGM equally contribute to the overall scattering signal, as expected for 1:1 mixture of non-interacting components, meaning that the emulsified nanoparticles do not engage interactions with the mucin chains of the matrix. In the case of TPGS-based NE, instead, only a fraction (37%) of the total signal of the NE was used to reconstruct the scattering from the mixture and a small downward deviation of the experimental curve is observed at low-q, possibly due to partial particle instability in presence of PGM. Contrarily to what reported by Zhang et al. [47], we do not observe particle aggregation as for the case of microemulsion-mucin interaction. Our observations are in line with previous experimental reports on PEG-coated drug delivery systems [9, 48-49] where nanoparticles with inert surface were observed to freely diffuse in the mucin matrix regardless of their size, provided that they are densely coated with low molecular weight PEG.

In **Fig. 3D** we report a similar analysis of the SAXS spectra when CS is added to the formulation. It is clear that the presence of CS has an impact on the structure of the matrix. A significant deviation of the linear-combination reconstruction from the experimental spectra is seen in the low-q region for all of the three systems. The largest discrepancy occurs for the Cremophor-based and Solutol-based NEs. The exceeding

intensity at low-q indicates that mucin aggregation occurs. CS-based drug delivery systems are retained by the mucus mesh mainly through electrostatic interactions with the negatively-charged mucins [50-51]. CS can interact with several mucin filaments grouping them in thick bundles around the trapped nanoparticles, thereby modifying the original mesh-spacing of mucus [51]. As previously discussed, such interactions can be also complemented by hydrogen bonding and hydrophobic forces when the two biopolymers are mixed in aqueous environment [16,52]. Indeed, the long-range electrostatic interactions are fully screened in SSNF conditions (i.e. high ionic strength), simulating the natural environment of the nasal mucosa. However, this does not prevent short-range mucin association. Here, the high affinity between the two biopolymers (CS and mucin) results in the local shrinking of the mucin gel network, creating larger pores between the CS-mucin bundles.

SAXS investigations clearly reveal that CS has an impact on the interaction of NEs with mucus. CS-free NEs do not interact with the PGM matrix. Only in the presence of added CS to the solution, interactions are promoted, inducing density unevenness in the mesh structure of mucins.

3.3 In vitro preliminary investigation of NEs biocompatibility

The biocompatibility of the three O/W NEs prepared was evaluated on macrophage-like cells obtained by differentiation of THP-1 human monocyte cells originally derived from acute monocytic leukaemia. Results are presented in **Fig. 4**.
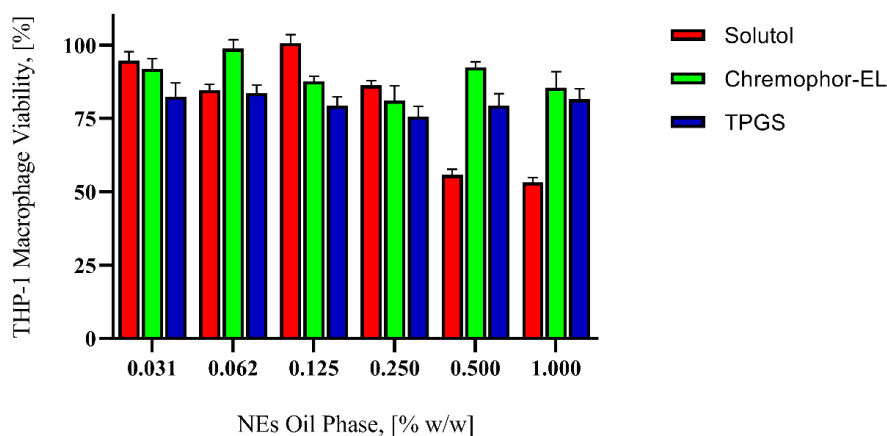

Fig. 4. THP-1 cells viability after 4 hours incubation with increasing concentrations of O/W NEs (blue, vitamin E TPGS based NE; green, macrogolglycerol ricinoleate based NE; red, PEG-12 15 hydroxystearate based NE). Data are presented as average and standard deviation of six replicates (n=6).

Macrophages were selected for this preliminary screening because they are part of the nasopharynx-associated lymphoid tissue (NALT) and are commonly present as particulate scavenging cells in the nasal tissue. Moreover, being phagocytic cells, they rapidly accumulate the nanocarrier *in vitro*. Data evidenced that the nanoemulsions presented in general good biocompatibility, with cell viabilities around or above 75%. In fact, both Chremophor and vitamin E-TPGS based NEs presented similar biocompatibility profiles, with no more than 25% of cells viability reduction at any concentration (minimum viability $81.04 \pm 5.05\%$ for Chremophor-

based NEs and 75.66 ± 3.53 for vitamin E-TPGS based NEs). Only in the case of Solutol-based NEs THP-1 cells viability was reduced to a value around 55% at the two highest NEs concentrations (53.19 ± 1.72 % at 1% w/w and 55.77 ± 1.93 % at 0.5% w/w). At higher dilutions, the percentage of cells survival was higher than 85% also in the case of Solutol-based NE (range 84.70-100.71%).

Considering that THP-1 monocyte were activated to behave like macrophages and that from the physicochemical properties the Solutol-based NE appears as the only one with an unequivocal positive surface charge (+11.8 ± 0.5 mV), an higher uptake of both nanoemulsion droplets and chitosan compared to the other formulations could account for the reduced viability observed for this specific O/W nanoemulsion.

This behaviour could be of interest in an application as vaccine adjuvant, since it has been reported that the action of O/W emulsions as vaccine adjuvants involve the recruitment and activation of immune cells and secretion of cytokines creating a local pro-inflammatory immune response [52]. Indeed, some nanosized adjuvants, such as liposomes and several types of nanoparticles, are classified as damage-associated molecular pattern (DAMP) inducers, since inducing a local and transient mucosal damage they cause the release of several stress factors classified as DAMPs recognized by the other epithelial cells and mucosal immune cells, triggering an innate immune response [53].

3.4 NEs diffusion in simulated mucus, followed by SAXS and SANS.

SAXS measurements were performed on NEs and admixed NE-mucin solutions, in order to clarify the structural properties of the NEs in contact with the mucus model. This allowed establishing the best suited formulations by the structural point of view, discarding TPGS-based NE, due to the formation of large particles that were not perfectly stable upon mixing with mucin. In the following, we propose a novel experimental approach based on SAXS and SANS, which permits following the penetration of NEs inside the PGM matrix by recording the structural changes associated to the evolution of the scattering patterns. Such an approach is complementary to the classical characterisation methods for particle diffusion [44, 54-58] and offers the unique advantage of direct evidence of the microscopic changes induced by the carriers when penetrating the gel matrix.

Diffusional studies were only focused on the Solutol-based formulation, as this NE presents the best suited features for a mucus-penetrating delivery formulation. In fact, as far as the structural properties are concerned, no dramatic difference was revealed between the Cremophor-EL and the Solutol-based formulations. Rather, the formulation containing Solutol, as evidenced with *in vitro* studies with activated THP-1 monocytes, presents an higher potential as mucosal vaccine adjuvant soliciting the innate immune response and was selected for further investigations.

SAXS and SANS diffusional experiment were designed to complement the above described structural studies by testing the ability of NEs to penetrate into the mesh-sieve constituted by the mucin network. According to the technique of choice, the best experimental conditions were selected in order to follow the nanoparticles entering the mucin matrix. In both cases, the network was diluted enough to allow the nanoparticles diffusing

across the mesh over distances (order of the mm) and on a timescale compatible with the structural experiments. Indeed, the absolute values of residence or diffusion times over real mucus barriers are not reproduced [60], but the propensity of the NEs to cross the mucosal barrier can be assessed.

For the SAXS experiments, 20 µl of NE formulations (c = 20% w/v) were carefully put in contact with 80 µl of PGM (c = 4% w/v) in a polycarbonate capillary (diameter = 2 mm), placed in a horizontal sample holder [see scheme in **Fig. A1** of **Appendix A**]. After 20 minutes, SAXS intensity was measured inside the PGM region at different distances from the PGM-NE interface. Results are reported in **Fig. 5 (panel A and B)**: both the formulations enter the mucin matrix, their intensity contribution to the total scattering becoming visible in the low and high q-region of the spectra, as expected (see the comparison between the scattering signals of PGM and NEs reported in **Fig. A2** of **Appendix A**). Approaching to the interface, we observe the presence of a larger amount of NEs (**Fig. 5**, from bottom up) in the matrix, and this is more pronounced in the presence of CS. The scattering signal of the two admixed systems of **Fig. 3** is also shown. A precise quantification of the amount of NEs diffusing at a given distance is out of the scope of this study and evidently, the experimental model does not faithfully reproduce the diffusion in physiological conditions. Nevertheless, we can clearly observe that the scattering intensity profiles of CS-free Solutol-based NE after 20 min contact didn't reach the admixed spectra (at 4% w/v NE) at any proximity to the interface. On the contrary, for the CS-added NE the intensity measured at a distance of about 10 mm from the interface is close to the SAXS profile of the admixed state. Therefore, we can conclude that more particles penetrate into the matrix and diffuse to a deeper extent in the presence of CS.
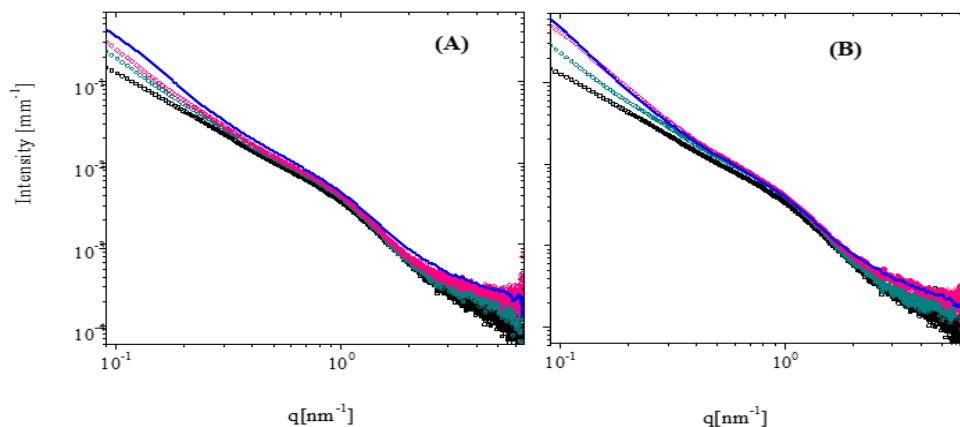

Fig. 5. Comparison between SAXS spectra relative to the diffusion experiments of Solutol-based O/W NEs CS-free **(panel A)** and CS-added **(panel B)** at different distances (d) from the PGM/NE interface: PGM (c=2% w/v, black squares), $d{\sim}20$ mm (green circles), $d{\sim}10$ mm (pink diamonds). The admixed spectra are also reported for reference (blue lines).

The results of the SAXS diffusion experiments were complemented by SANS analogous investigations. Compared to SAXS, SANS better highlights the scattering contributions from the cysteine-rich regions of the glycoprotein, which are thought to be responsible for the dense porous structure of mucin gel (**Fig. 3B**). Moreover,

SANS allows investigating structural changes on long time scale without inducing radiation damage. Here, the NEs (c = 20 % w/v) were gently loaded in a quartz cell on top of the PGM matrix (c =10 % w/v) [see scheme in **Figure A.1** of **Appendix A**] and SANS spectra were recorded at a fixed position below the interface (measuring area ~0.4 cm^2) within the PGM matrix, at different delays. The progressive penetration of the NEs in the observation region was followed for 24 hours.

In **Fig. 6**, the two series of spectra correspond to the time evolution of the structure of the PGM matrix during the diffusion of the NEs, CS-free and CS-added (**panel A** and **B**, respectively). The spectra of the pure PGM matrix (black open dots) is also reported. The scattering signals at the equal delay evolve from that of the pure PGM matrix. As for SAXS, both the NEs, with and without CS, do no stay phase separated, but the progressive penetration of the nanocarriers into the PGM matrix is revealed by the increase of the scattered signal and by the change of the intensity profile, occurring on a faster time scale in the presence of CS. In particular, the typical structure peak at q ~0.25nm^{-1} disappears more rapidly for the CS-added NE. In the CS-free NE, a broadening of the peak is observed which also seems to shift towards lower-q values, suggesting that, upon contact with the naked NE solution, the mesh size of the matrix gets slightly larger. Indeed, muco-inert nanoparticles of size comparable to the mucus pore can experience steric interactions with the mesh [59]. On the contrary, for mucus-interacting nanoparticles, namely the CS-added NE, there is an evident loss of correlation in the mucin matrix, and the rapid disappearance of the structure peak is accompanied by an enhanced penetration of the particles into the mucin network. These results suggest that the CS chains tightly bind to mucin, eventually leading to the collapse of the gel via the formation of condensed bundles and larger channels, allowing for faster diffusion of the drug vehicles. In many works, CS-coated nanovehicles have been observed to be trapped into the mucus [60], their crossing of the full thickness of the mucus layer being hindered and thus their uptake reduced. In our case, CS is not permanently bound to the NE surface, so while interacting with mucins, it does not retain the NE droplets. On the contrary, the NEs are facilitated in slipping through the larger gaps opened between the bunches of CS chains and mucin.
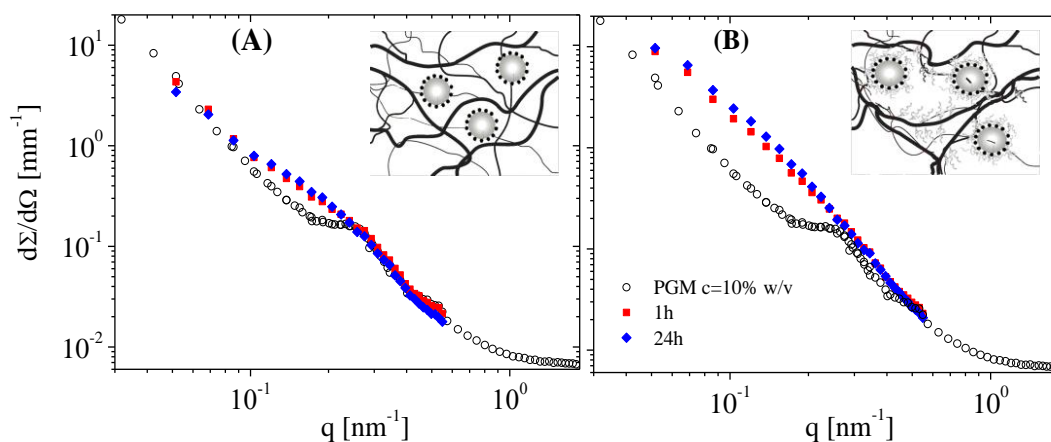

Fig. 6. Comparison between SANS spectra relative to the diffusion experiments of Solutol-based O/W NEs, CS-free **(panel A)** and CS-added **(panel B)**. As the diffusion proceeds, the SANS spectra evolve from bottom up. Sketches of the different features of the diffusion processes occurring in the presence or absence of CS are also shown.

3.5 In vitro cellular uptake in primary phagocytic cells

In vitro experiments were conducted on swine monocyte-derived macrophages in order to evaluate the uptake of the O/W Solutol-based NE in primary cells instead of immortalized cells. In **Fig. 7,** the comparison between macrophages without lipid inclusions due to uptake of NE (**panel A**) and macrophages presenting lipid inclusions or vesicles (black arrows, **panel B**) due to the nanoemulsion uptake is shown. As hypothesized from data obtained with THP-1 cells, the NE droplets were avidly taken up by the phagocytic cells already after 2 hours contact; nevertheless, the number of dead cells up to 12 hours was not different from the one of the control (10%), probably because of the higher dilution of the NE (0.02% w/w) compared to the experiments carried out with THP-1 cells. Nevertheless, an increase of dead cells (up to 80%) was observed only after prolonged exposure (24 hours), suggesting that the proposed formulation could be further studied as an innovative mucus penetrating and biocompatible nanoadjuvant for mucosal vaccination.
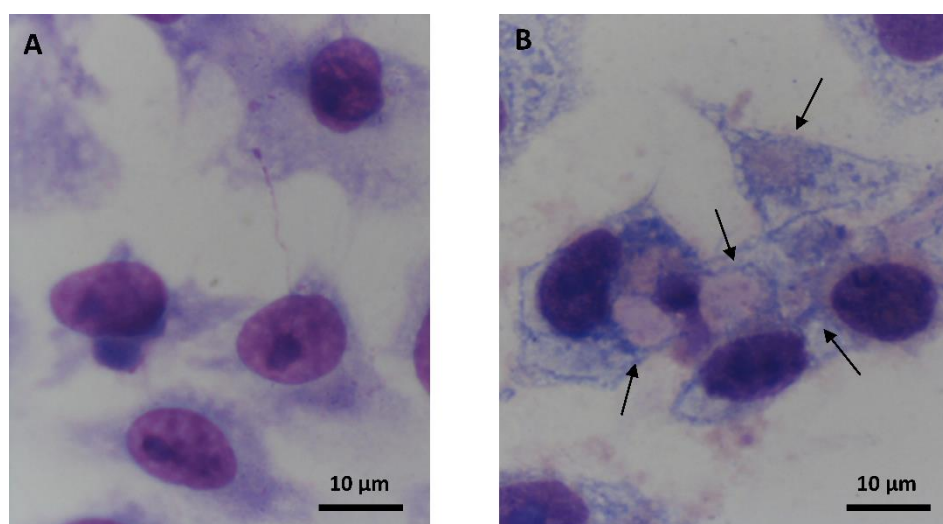

Fig. 7. Digital images of swine monocyte-derived macrophages without lipid inclusions due to uptake of NE (**panel A**) and with macrophages presenting lipid inclusions or vesicles (black arrows, **panel B**) due to the nanoemulsion uptake. A number of phagosomes can be identified inside the cells, but no apparent toxicity was evidenced up to 12 hours.

4. Conclusions

Mucosal barriers act as physiological filters, regulating the diffusion of bacteria, virus, environmental particles and drug carriers, with size spanning from the nanometer to the micron range. Beside size-exclusion mechanisms, mucus can slow down the diffusion of molecules by physico-chemical interactions, including electrostatic and hydrophobic binding. To avoid entrapment and consequent slow diffusion, nanovectors are engineered with different functionalized surfaces with the aim to minimize the local interactions with the mucin glycoproteins matrix or induce local disruption of the pores/channels gel structure (mucolytic agents).

Here, we presented a detailed structural study of novel O/W NE formulations, including PEGylated surfactants to be used as potential nanovectors for nasal administration, with and without added CS, as mucus-modulating agent. The NEs have been characterized and studied for their interaction with commercial purified porcine gastric mucins, a model system for the nasal secretions. As a distinctive feature, CS was not grafted to the surface of the NEs but it was used in co-association with the nanoformulation. SAXS investigations allowed for the selection of the structurally most promising formulations, while diffusional SAXS and SANS experiments were designed to assess the propensity of the selected formulations, with or without added CS as adjuvant, to enter the mucus. CS addition was found to confer to the formulation the desired property of facilitating the delivery of the NEs through the mucin network barrier. In fact, CS-free PEG-coated NEs did not interact with mucins. Reversely, in the presence of CS, a modification of the local structure of the gel mucin matrix was observed together with an enhanced penetration of the NEs through it. This is likely to be driven by preferential electrostatic interactions between the two biopolymers, inducing density unevenness in the network with the formation of condensed bundles and larger pores, as previously speculated by Menchicchi *et al.* [16], which let the nanoparticles free to move. In reason of the nanoemulsions formulation and structure, during the transmucosal delivery of drugs or vaccines, the particles are not trapped in the mucus but facilitated to cross the mucosal barriers. Furthermore, the formulations were tested in presence of activated human monocytes showing good biocompatibility and Solutol-based NE was demonstrated to be avidly taken up by porcine peripheral blood mononuclear cells. The selected formulation appears promising as an innovative nanoadjuvant system for nasal vaccination and *in vivo* studies are ongoing to substantiate this claim.

References.

[1] A. Gupta, H. B. Eral, T. A. Hattona P. S. Doyle, Soft Matter 12, (2016), 2826-2841.

[2] Y. Singh, J. G. Meher, K. Rava, F. Ali Khan, M. Chaurasia, N. K. Jain, M. K. Chourasia, Journal of Controlled Release 252, (2017), 28–49.

[3] M. Jaiswal, R. Dudhe, P. K. Sharma Biotechnology 5, (2015),123–127.

[4] C. Comfort, G. Garrastazu, M. Pozzoli, F. Sonvico, Current Topics in Medical Chemistry 15, (2015), 356–368.

[5] S. K.S. Kushwaha, R. K. Keshari, A.K. Rai, Journal of Applied Pharmaceutical Science 1(7), (2011), 21-28.

[6] A. Clementino, M. Batger, G. Garrastazu, M. Pozzoli, E. Del Favero, V. Rondelli, B. Gutfilen, T. Barboza, M.B. Sukkar, S.A.L. Souza, L. Cantù, F. Sonvico, International Journal of Nanomedicine 11, (2016), 6575-6590.

[7] A U. Bielinska, P. E. Makidon, K. W. Janczak, L. P. Blanco, B. Swanson, D. M. Smith, T. Pham, Z. Szabo, J. F. Kukowska-Latallo, J. R. Baker, Jr., Journal of Immunology 192(6), (2014), 2722-2733.

[8] H.R. Costantino, L. Illum, G. Brandt, PH Johnson, SC. Quay, International Journal of Pharmaceutics 337, (2007), 1-24.

[9] O. Lieleg, K. Ribbeck, Trends in Cell Biology 21(9), (2011), 543-551.

[10] J. Leal, H.D.C. Smyth, D. Ghosh, International Journal of Pharmaceutics 532, (2017), 555–572.

[11] T. A. Ahmed, B. M Aljaeid, Drug Design, Development and Therapy 10, (2016), 483–507.

[12] C. Saikia, P. Gogoi, T. K Maji, Journal of Molecular and Genetic Medicine S4:006 (2015).

[13] A. R. Mackie, F. M. Goycoolea, B. Menchicchi, C. M. Caramella, F. Saporito, S. Lee, K. Stephansen, I. S. Chronakis, M. Hiorth, M. Adamczak, M. Waldner, H. M. Nielsen, L. Marcelloni, Macromolecular Bioscience 17(8), (2017), 1600534.

[14] G. Sandri, S. Motta, M.C. Bonferoni, P. Brocca, S. Rossi, F. Ferrari, V. Rondelli, L. Cantù, C. Caramella, E. Del Favero, European Journal of Pharmaceutics and Biopharmaceutics 110, (2017), 13-18.

[15] F. Sonvico, A. Clementino, F. Buttini, G. Colombo, S. Pescina, S. Stanisçuaski Guterres, A. Raffin Pohlmann, S. Nicoli, Pharmaceutics 10(1), (2018), 34–34.

[16] B. Menchicchi, J. P. Fuenzalida, K. B. Bobbili, A. Hensel, M. J. Swamy, F. M. Goycoolea, *Biomacromolecules* 15, (2014), 3550-3558.

[17] I.A. Sogias, A. C. Williams, V. V. Khutoryanskiy, Biomacromolecules 9, (2008),1837 − 1842.

[18] C.M. Lehr, J. A. Bouwstra, E. H. Schacht, H. E. Junginger, International Journal of Pharmaceutics 78, (1992), 43 − 48.

[19-20] S. Rossi, F. Ferrari, M.C. Bonferoni, C. Caramella, European Journal of Pharmaceutical Sciences 10, (2000), 251 − 7; 12, (2001), 479 − 85.

[21] B. Menchicchi, J. P. Fuenzalida, A. Hensel, M. J. Swamy, L. David, C. Rochas, F. M. Goycoolea, Biomacromolecules 16, (2015), 924 − 935.

[22] K. E. Haugstad, A. G. Håti, C. T. Nordgård, P. S. Adl, G. Maurstad, M. Sletmoen, K. I. Draget, R. S. Dias, B. T. Stokke, Polymers 7 (2015), 161-185.

[23] T. Narayanan, H. Wacklin, O. Konovalov, R. Lund, Crystallography Review 23, (2017), 160-226.

[24] D. Snary, A. Allen, Biochemical Journal, 123, (1971), 845-853.

[25] X. Cao, R. Bansil, K R. Bhaskar, B. S Turner, J T. LaMont, N. Niu, N. H Afdhal, Biophysical Journal 76, (1999), 1250-1258

[26] Y.Y. Wang, S.K. Lai, J.S. Suk, A. Pace, R. Cone, J. Hanes, Angewandte Chemie International Edition 47, (2008), 9726–9729.

[27] C. T. Nordgård, K. I. Draget, Advanced Drug Delivery Reviews 124, (2018), 175–183.

[28] T. Narayanan, M. Sztucki, P. Van Vaerenbergh, J. Léonardon, J. Gorini, L. Claustre, F. Sever, J. Morse, P. Boesecke, Journal of Applied Crystallography 51(6), (2018), 1511-1524.

[29] A. Brulet, D. Lairez, A. Lapp, J.P. Cotton, Journal of Applied Crystallography 40, (2007), 165-177.

[30] L. Shi, F. Carn, F. Boue, G. Mosser, E. Buhler, Soft Matter 9 (20), (2013), 5004-5015.

[31] J. Puig-Rigall, I. Grillo, C. A. Dreiss, G. Gonzalez-Gaitano, Langmuir 33, (2017), 4737 − 4747.

[32] T. Narayanan, Current Opinions in Colloid Interface Science 14, (2009), 409–415.

[33] A. Guinier, G. Fournet, Small-Angle Scattering of X-Rays, John Wiley and Sons, New York, (1955).

[34] J. Penser, S. Krueger, C. P. Adams, J. Katsarasa, Journal of Applied Crystallography 39, (2006), 293.

[35] M. Kotlarchyk and S.-H. Chen, Journal of Chemical Physics 79, (1983), 2461.

[36] Y. Guo, Jun Luo, S Tan, B O Otieno, Z. Zhang, European Journal of Pharmaceutical Sciences 49(2), (2013), 175-186.

[37] H. Gelderblom, J. Verweij, K. Nooter, A. Sparreboom, European Journal of Cancer 37, (2001), 1590-1598.

[38] P. Debye, H. R. Anderson and H. Brumberger, Journal of Applied Physics 28, (1957), 679.

[39] C. L. Dora, L. F. C. Silva, J-L. Putaux, Y. Nishiyama, I. Pignot-Paintrand, R. Borsali, E. Lemos-Senna, Journal of Biomedical Nanotechnology. 8(2), (2012),1-9.

[40] E. Buhler, M. Rinaudo, Macromolecules 33, (2000), 2098–2106.

[41] L. Shi, F. Carn, F. Boué, E. Buhler Physical Review E 94, (2016), 032504.

[42] R. Bansil, B. S. Turner, Current Opinion in Colloid & Interface Science 11, (2006),164 − 170.

[43] Y. Z. Falk, J. Engblom, J.S. Pedersen, T. Arnebrant, V. Kocherbitov, Journal of Physical Chemistry B 122 (2018), 7539.7546.

[44] P. C. Griffiths, P. Occhipinti, C. Morris, R. K. Heenan, S. M. King, M. Gumbleton. Biomacromolecules 11, (2010), 120–125.

[45] E. Di Cola, G. E. Yakubov, T. A. Waigh, Biomacromolecules 9, (2008), 3216-3222.

[46] T. A. Waigh, A. Papagiannopoulos, A. Voice, R. Bansil, A.P. Unwin, C.D. Dewhurst, B. Turner, N. Afdhal, Langmuir 18, (2002), 7188–7195.

[47] J. Zhang, Y. Lv, B. Wang, S. Zhao, M. Tan, G. Lv, X. Ma, Molecular Pharmaceutics 12, (2015), 695-705.

[48] L. Wu, W. Shan, Z. Zhang, Y. Huang, Advanced Drug Delivery Review 124, (2018), 150-163.

[49] J. T. Huckaby, S. K. Lai Advanced Drug Delivery Review 124, (2018), 125-139.

[50] X. Murgia, B. Loretz, O. Hartwig, M. Hittinger, C-M Lehr, Advanced Drug Delivery Review 124, (2018), 82-97.

[51] E. Y. T. Chen, Y.-C. Wang, C.-S. Chen, W.-C. Chin, PLOSone, 5(11), (2010), e15434.

M. Collado-González, Y. González Espinosa and F. M. Goycoolea. Interaction Between Chitosan and Mucin: Fundamentals and Applications, Biomimetics (2019) 4, 32-54

[52] Bastola R, Noh G, Keum T, Bashyal S, Seo JE, Choi J, Oh Y, Cho Y, Lee S. Vaccine adjuvants: smart components to boost the immune system. Arch Pharm Res. 2017; 40(11):1238-1248. doi: 10.1007/s12272-017-0969-z

[53] Aoshi T. Modes of Action for Mucosal Vaccine Adjuvants. Viral Immunol. 2017;30(6):463-470. doi: 10.1089/vim.2017.0026

[54] J. M. Newbya, I. Seima, M. Lysyb, Y. Ling, J. Huckaby, S. K. Lai, M. G. Forest, Advanced Drug Delivery Review 124, (2018), 64-81.

[55] B.S. Schuster, L.M. Ensign, D.B. Allan, J.S. Suk, J. Hanes, Advanced Drug Delivery Review 91, (2015),70–91.

[56] J. Grießinger, S. Dünnhaupt, B. Cattoz, P. Griffiths, S. Oh, S. Borrós i Gómez, M. Wilcox, J. Pearson, M. Gumbleton, A. Bernkop-Schnürch, European Journal of Pharmaceutics and Biopharmaceutics 96, (2015), 464-476.

[57] S.K. Lai, Y.-Y. Wang, J. Hanes, Advanced Drug Delivery Review 61, (2009),158–171.

[58] M. Liu, J. Zhang, W. Shan, Y. Huang Asian Journal of Pharmaceutical Sciences 10, (2015), 275-282.

[59] A.G. Beule, Current Topics in Otorhinolaryngology - Head and Neck Surgery 9, ISSN (2010), 1865-10.

[60] A. Mistry, S. Stolnik, L. Illum, International Journal of Pharmaceutics 379(1), (2009), 146-157.